

# Retaining Short-term Variability Reduces Mean State Biases in Wind Stress Overriding Simulations

Matthew T. Luongo<sup>1</sup>, Noel Brizuela<sup>2</sup>, Ian Eisenman<sup>3</sup>, and Shang-Ping Xie<sup>4</sup>

<sup>1</sup>University of California, San Diego

<sup>2</sup>Scripps Institution of Oceanography

<sup>3</sup>UC San Diego

<sup>4</sup>UCSD

December 6, 2023

1 **Retaining Short-term Variability Reduces Mean State**  
2 **Biases in Wind Stress Overriding Simulations**

3 **Matthew T. Luongo<sup>1</sup>, Noel G. Brizuela<sup>1,2</sup>, Ian Eisenman<sup>1</sup>, & Shang-Ping Xie<sup>1</sup>**

4 <sup>1</sup>Scripps Institution of Oceanography, UC San Diego, La Jolla, CA

5 <sup>2</sup>Lamont-Doherty Earth Observatory, Columbia University, New York, NY

6 **Key Points:**

- 7 • Most previous wind stress overriding simulations have disabled momentum feed-  
8 backs in global climate models by overriding with a climatology
- 9 • We introduce a protocol to override with interannually varying wind stress, which  
10 leads to smaller biases than climatological overriding
- 11 • We attribute this difference to a lack of synoptic variability in climatological over-  
12 riding which shoals the mixed layer

---

Corresponding author: M.T. Luongo, [mluongo@ucsd.edu](mailto:mluongo@ucsd.edu)

**Abstract**

Positive feedbacks in climate processes can make it difficult to identify the primary drivers of climate phenomena. Some recent global climate model (GCM) studies address this issue by controlling the wind stress felt by the surface ocean such that the atmosphere and ocean become mechanically decoupled. Most mechanical decoupling studies have chosen to override wind stress with an annual climatology. In this study we introduce an alternative method of interannually varying overriding which maintains higher frequency momentum forcing of the surface ocean. Using a GCM (NCAR CESM1), we then assess the size of the biases associated with these two methods of overriding by comparing with a freely evolving control integration. We find that overriding with a climatology creates sea surface temperature (SST) biases throughout the global oceans on the order of  $\pm 1^\circ\text{C}$ . This is substantially larger than the biases introduced by interannually varying overriding, especially in the tropical Pacific. We attribute the climatological overriding SST biases to a lack of synoptic and subseasonal variability, which causes the mixed layer to be too shallow throughout the global surface ocean. This shoaling of the mixed layer reduces the effective heat capacity of the surface ocean such that SST biases excite atmospheric feedbacks. These results have implications for the reinterpretation of past climatological wind stress overriding studies: past climate signals attributed to momentum coupling may in fact be spurious responses to SST biases.

**Plain Language Summary**

Because the ocean influences the atmosphere and vice versa, chicken-or-egg type problems abound throughout the climate system. Some studies have addressed this by controlling the wind stress field felt by the ocean in climate models in order to mechanically decouple the ocean from the atmosphere and thus determine the surface ocean response to a change in momentum forcing. Most previous studies that override wind stress have fed the ocean a mean annual cycle; however, this method removes the effect of shorter-term events like storms. We compare how well overriding experiments, forced either with the mean annual cycle of wind stress or with year-to-year varying wind stress, agree with a freely evolving control simulation. We find substantially larger sea surface temperature (SST) biases in the simulation forced with the mean annual cycle of wind stress. We attribute these biases to the lack of short-term weather events which mix the surface ocean.

## 1 Introduction

Comprehensive global climate model (GCM) simulations of the coupled atmosphere-ocean system have been used to study the response of the climate to external forcings and to understand intrinsic modes of climate variability. However, interpreting results from comprehensive coupled GCMs is complex and can often give rise to chicken-or-egg problems, especially regarding whether the atmosphere is driving the ocean or vice versa. Often the answer is that both are driving each other. Employing a hierarchy of models, from the simplest two-layer quasi-geostrophic models to the most complex GCMs, and peeling off subsequent levels of complexity until one arrives at the simplest configuration which explains the process of interest, is seen as the gold standard for bridging the gap between simulation and understanding (Held, 2005).

Many studies throughout the past two decades have highlighted the gap in the hierarchy of models between a comprehensive GCM where the atmosphere and ocean are dynamically coupled (AOGCM) and an atmospheric GCM that is thermodynamically coupled to a motionless mixed layer slab ocean model (e.g., Green & Marshall, 2017; Kang et al., 2020). The difference between these two modeling configurations might naïvely be considered the impact of atmospheric momentum forcing on the ocean. However, because the ocean dynamically responds to fluxes of both buoyancy and momentum, an intermediate step exists where the ocean is able to respond to anomalous fluxes of either buoyancy or momentum only and then feed back on the atmosphere. Recently, modeling studies have explored this niche through the use of partially decoupled GCM simulations where a certain flux into the ocean is specified rather than allowed to freely evolve.

The specific process of overriding wind stress such that the ocean cannot react to the freely evolving wind field, and thus the ocean is “mechanically decoupled” (Larson & Kirtman, 2015), is a common GCM partial decoupling approach. Despite the specified surface momentum flux, the ocean is still able to dynamically respond to anomalous buoyancy fluxes; as a result, wind stress overriding simulations sit squarely between fully coupled and slab ocean GCM studies and have played a central role in investigating how buoyancy and momentum forcing affect the ocean and climate system. This specific process of partially decoupling the ocean from the atmosphere via momentum forcing is variously referred to in the literature as “mechanical decoupling” or “wind stress overriding,” and we use these terms interchangeably.

76 Mechanically decoupled simulations were initially used primarily to study the im-  
77 pact of El Niño-Southern Oscillation (ENSO) on the climate system because of the cru-  
78 cial role of mechanical coupling between wind stress and thermocline depth in the Bjer-  
79 knes feedback (Bjerknes, 1969; Wyrski, 1975). In a series of studies, Larson and Kirtman  
80 (2015, 2017, 2019) effectively suppressed ENSO variability by globally overriding sur-  
81 face ocean wind stress with a daily climatology (i.e., a day-of-year average across mul-  
82 tiple years) to create a set of initial conditions without ENSO influences in order to study  
83 how coupled instabilities may lead to subsequent ENSO growth.

84 More recently, however, global climatological wind stress overriding has been used  
85 to study non-ENSO phenomena. These studies explore topics such as Pacific sea surface  
86 temperature (SST) variance (Larson, Vimont, et al., 2018), buoyancy-forced character-  
87 istics of the Atlantic Meridional Overturning Circulation (AMOC, Larson et al., 2020),  
88 cross-equatorial energy transport (F. Liu et al., 2021), extratropical atmospheric vari-  
89 ability (Larson, Pegion, & Kirtman, 2018; Larson et al., 2022), and global warming (McMonigal  
90 et al., 2023). Other studies have explored similar topics including the Pacific Meridional  
91 Mode (PMM) and Indian Ocean meridional heat transport by overriding the wind stress  
92 with a climatology in the Equatorial Pacific only and allowing the wind stress to freely  
93 evolve elsewhere (Zhang et al., 2021; McMonigal & Larson, 2022).

94 While the vast majority of wind stress overriding simulations have used climato-  
95 logical overriding of some form, as described above, other schemes have also been occa-  
96 sionally used, such as overriding with wind stress from a repeating ENSO cycle (Larson  
97 & Kirtman, 2019) or adding specified anomalies to a climatology (Chakravorty et al.,  
98 2020, 2021). Other studies have supplied daily, interannually varying wind stress to the  
99 ocean from a separate integration where daily wind stress is output (Lu & Zhao, 2012;  
100 W. Liu et al., 2015, 2018; Luongo et al., 2022a, 2023; Fu & Fedorov, 2023). As opposed  
101 to overriding the total wind stress field in one model as discussed above, the flux anomaly  
102 forced model intercomparison project (FAFMIP: Gregory et al., 2016) specifies momen-  
103 tum anomalies to different model control states.

104 Overriding wind stress to decouple the ocean from the atmosphere invariably cre-  
105 ates a climate bias relative to a control integration. We refer to this signature as the “de-  
106 coupling bias.” The question then arises as to how these wind stress overriding schemes  
107 differ in the size and pattern of their decoupling biases. In this study, we explore the ex-

108 tent to which the adopted decoupling scheme alone impacts the climate system. We fo-  
109 cus primarily on climatological overriding, since this is the main decoupling protocol used  
110 in previous studies. We primarily present results from two GCM simulations meant to  
111 systematically explore the bias associated with each decoupling protocol compared with  
112 a freely evolving, fully coupled control case.

113 This paper is laid out as follows. Section 2 explains wind stress overriding meth-  
114 ods, discusses the smoothing effects of climatological averaging on wind stress variabil-  
115 ity, and describes the GCM simulations used in this study. Section 3 describes the SST  
116 biases associated with the two overriding approaches and proposes possible drivers of the  
117 differences. We discuss implications for the results of past wind stress overriding stud-  
118 ies in Section 4 and conclude in Section 5.

## 119 **2 Wind Stress Overriding Simulations**

120 We use the Community Earth System Model, Version 1.2 (CESM1: Hurrell et al.,  
121 2013) from the National Center for Atmospheric Research in its standard fully coupled  
122 configuration, which includes active atmosphere (CAM5: Neale et al., 2010), ocean (POP2:  
123 Smith et al., 2010), land surface (CLM4: Lawrence et al., 2012), and sea ice (CICE4: Hol-  
124 land et al., 2012) components that are interactively coupled by the model’s coupler (Craig,  
125 2014). Many previous wind stress overriding studies have also used versions of CESM  
126 (Larson & Kirtman, 2015; Larson et al., 2017; Larson, Vimont, et al., 2018; Larson et  
127 al., 2020; Chakravorty et al., 2020, 2021; F. Liu et al., 2021; McMonigal & Larson, 2022;  
128 Luongo et al., 2022a, 2023; McMonigal et al., 2023; Fu & Fedorov, 2023). In this study,  
129 we adopt the configuration used in Luongo et al. (2022a, 2023): the model is forced with  
130 standard pre-industrial forcing, and the atmosphere and land are run on a nominal 2°  
131 grid while the ocean and sea ice are run on a nominal 1° grid. Note that the model cal-  
132 endar has no leap years. We run one 51-year simulation, “Ctrl,” in a fully coupled con-  
133 figuration and output daily wind stress for the subsequent overriding experiments, as ex-  
134 plained below. We consider Ctrl as the reference “truth” throughout this study.

135 The basic concept of wind stress overriding and how it differs from a fully coupled  
136 model evolution is laid out schematically in Figure 1. At each coupling step in a fully  
137 coupled run, the ocean and atmosphere component models pass their state to the GCM  
138 coupler, which then computes buoyancy and momentum fluxes and passes them back to

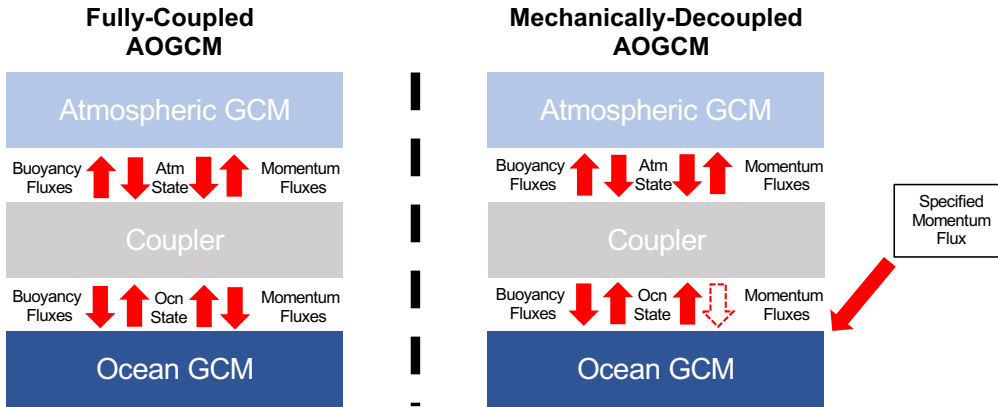


**Figure 1.** Schematic illustrating the difference between a fully coupled Atmosphere-Ocean-GCM (AOGCM) and a mechanically-decoupled AOGCM. In wind stress overriding experiments, the handoff between the coupler and the ocean is interrupted and the ocean is instead fed a specified momentum flux. All other flux coupling is retained.

139 the component models. Ocean coupling occurs daily in CESM. This hand-off between  
 140 the coupler and the ocean is partially interrupted in wind stress overriding simulations  
 141 such that the ocean is instead forced with a specified momentum flux field. While in prin-  
 142 ciple one could alternatively approximately override wind stress by intercepting the hand-  
 143 off from the atmosphere to the coupler before momentum fluxes are computed (W. Liu  
 144 et al., 2018), most studies directly override in the ocean component to avoid any unwanted  
 145 downstream effects. It should be noted that wind stress overriding only affects momen-  
 146 tum fluxes into the ocean; turbulent heat fluxes, which use wind speed in bulk formu-  
 147 lation, are retained as thermal fluxes into the surface ocean.

148 **2.1 Climatological Overriding**

Climatological overriding is the method most often employed to override wind stress  
 in mechanical decoupling experiments. The basic assumption of climatological overrid-  
 ing is one of approximate linearity and can be stated as

$$\langle F(\vec{\tau}) \rangle \approx F(\langle \vec{\tau} \rangle) . \tag{1}$$

149 Here angle brackets denote a climatological time averaging process to create a mean an-  
 150 nual cycle from a multi-year record. Equation 1 indicates that the mean state of the cli-  
 151 mate,  $F$ , which is a function of wind stress,  $\vec{\tau}$ , is approximately equal to the state of cli-

Simulation Name	$\vec{\tau}$ Overriding Protocol
Ctrl	N/A: Freely evolving control case
ClimTau	Override wind stress with 50-year climatology.
FullTau	Override wind stress with interannually varying field.
ENSONeutralTau	Override wind stress with repeating neutral ENSO year.
ENSONegativeTau	Override wind stress with repeating negative ENSO year.
ENSOPositiveTau	Override wind stress with repeating positive ENSO year.

**Table 1.** The simulation name and description of the six simulations considered in this study. We primarily focus on the difference in the 50-year average climate response between each overriding method (Rows 2-6) and the fully coupled control case (Row 1). The specific years used in ENSONeutralTau, ENSONegativeTau, and ENSOPositiveTau are chosen based on the Nino 3.4 regional SST anomaly in Ctrl and are shown in Figure S3.

152 mate as a function of mean wind stress. We take the day-of-year average of daily wind  
 153 stress data from years 1-50 of the Ctrl run to create a daily climatology of global wind  
 154 stress. The “ClimTau” simulation is forced with this daily climatology for 50 years.

## 155 2.2 Interannually Varying Overriding

156 Taking a daily climatology averages out high frequency variability. The climatol-  
 157 ogy retains the mean seasonal cycle, but synoptic and subseasonal variability are largely  
 158 averaged out. This higher frequency wind stress forcing, which includes phenomena such  
 159 as storms, may have important impacts on the mean ocean state due to processes such  
 160 as upper ocean mixing (e.g., Brizuela et al., 2023). The degree to which Equation 1 fails  
 161 to apply represents the degree of nonlinear rectification in the climate system (e.g., Huy-  
 162 bers & Wunsch, 2003; Eisenman, 2012), i.e., the extent to which higher-frequency wind  
 163 stress variability projects onto the longer-term ocean state.

164 Luongo et al. (2022a, 2023) used wind stress overriding to study the quasi-equilibrium  
 165 upper ocean response to extratropical top-of-atmosphere aerosol-like radiative forcing.  
 166 The authors mechanically decoupled the ocean from the atmosphere by overriding with  
 167 a time evolving multi-year daily wind stress field, thereby maintaining full wind stress

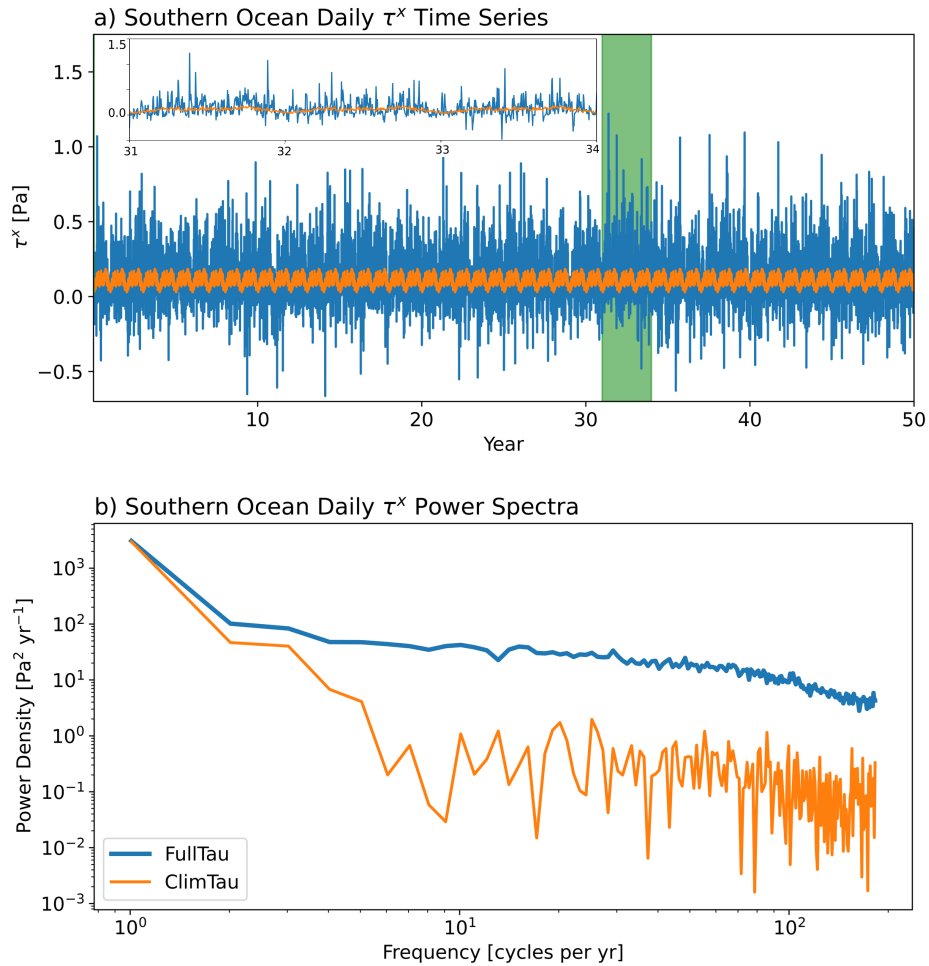


**Figure 2.** a) Time series of daily zonal wind stress,  $\tau^x$ , from a specific location in the Southern Ocean ( $60^\circ\text{S}$ ,  $25^\circ\text{W}$ : yellow star in Figure 3b) for FullTau (blue) and ClimTau (orange). Years 31-34 of the simulation are highlighted in the inset. b) Power spectrum of daily zonal wind stress for FullTau and ClimTau. Both spectra are computed using Bartlett's Method by taking the average of one-year periodograms for each of the fifty years.

168 variability. Here we replicate this overriding scheme in the “FullTau” simulation. Note  
 169 that wind stress in year  $n$  of the FullTau simulation is taken from year  $n + 1$  of Ctrl,  
 170 and that the 50-year FullTau simulation, which has the wind stress field specified from  
 171 years 2-51 of Ctrl, is equivalent to the “Tau1S1” simulation in Luongo et al. (2022a). The  
 172 one-year offset is imposed in order to circumvent the issue that if year  $n$  of FullTau was  
 173 given wind stress from year  $n$  of Ctrl, then the two simulated climates would be precisely  
 174 equal due to CESM’s bit-for-bit reproducibility and the fact that our wind stress over-  
 175 ridding technique is exact. Disrupting the temporal covariance between the atmosphere  
 176 and ocean causes FullTau to be mechanically decoupled. All simulations analyzed in this  
 177 study are described in Table 1.

178 This interannually varying overriding method requires management of daily wind  
 179 stress fields for the full duration of the target overriding simulation, whereas climato-  
 180 logical overriding requires management of just one year of wind stress fields. However,  
 181 in our case of standard resolution CESM on the Cheyenne supercomputing system, the  
 182 storage cost for 51 years of daily coupler files from Ctrl, which includes all surface flux  
 183 fields passed from the coupler to the ocean, is 650 GB. This is less than the storage cost  
 184 for the monthly atmospheric and ocean data fields generated by the 51 year Ctrl (720  
 185 GB).

186 Figure 2a plots the zonal component of daily wind stress,  $\tau^x$ , at a specific location  
 187 in the Southern Ocean (60°S, 25°W: yellow star in Figure 3b) for FullTau (blue) and ClimTau  
 188 (orange). The daily values of  $\tau^x$  in FullTau vary considerably on daily to interannual timescales,  
 189 while the variability of  $\tau^x$  in ClimTau is markedly suppressed with strong wind stress  
 190 events associated with weather essentially removed. Frequency spectra (Figure 2b) fur-  
 191 ther describe the difference between FullTau and ClimTau. We use Bartlett’s Method  
 192 to compute the spectra of  $\tau^x$  in both FullTau and ClimTau: we compute the periodogram  
 193 for each year in the 50-year span (after removing the mean and linear trend from the full  
 194 time series), and then we take the average of the 50 spectra. The power spectra of these  
 195 two Southern Ocean  $\tau^x$  time series clearly show that ClimTau exhibits substantially less  
 196 energy across timescales than FullTau. Unsurprisingly, there is a stark difference in wind  
 197 stress variance between the two simulations throughout the Southern Ocean and in vast  
 198 areas of the North Atlantic and North Pacific as well (Figure 3a & b). As discussed fur-  
 199 ther in Section 3.2, the lack of temporal variability in ClimTau indicates that the sur-

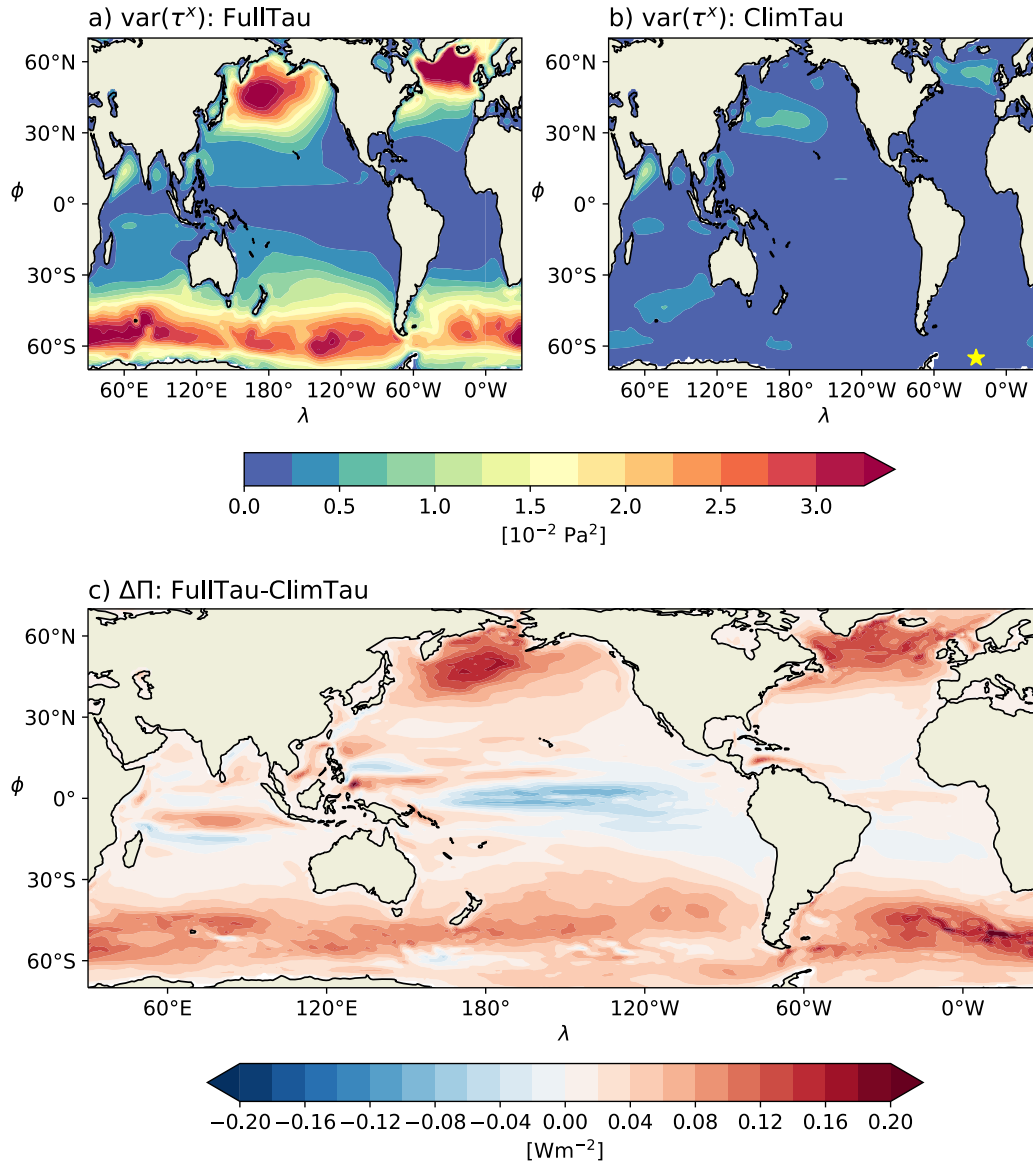


**Figure 3.** Top row: Variance in daily zonal wind stress,  $\tau^x$ , in FullTau (a) and ClimTau (b). The yellow star in panel b indicates the location of the data presented in Figure 2. Bottom row: Difference in wind work,  $\Pi$ , between the FullTau and ClimTau simulations.

200 face ocean will receive less kinetic energy flux in the case of climatological wind stress  
 201 overriding than it otherwise would in Ctrl.

### 202 3 Results

#### 203 3.1 SST Response

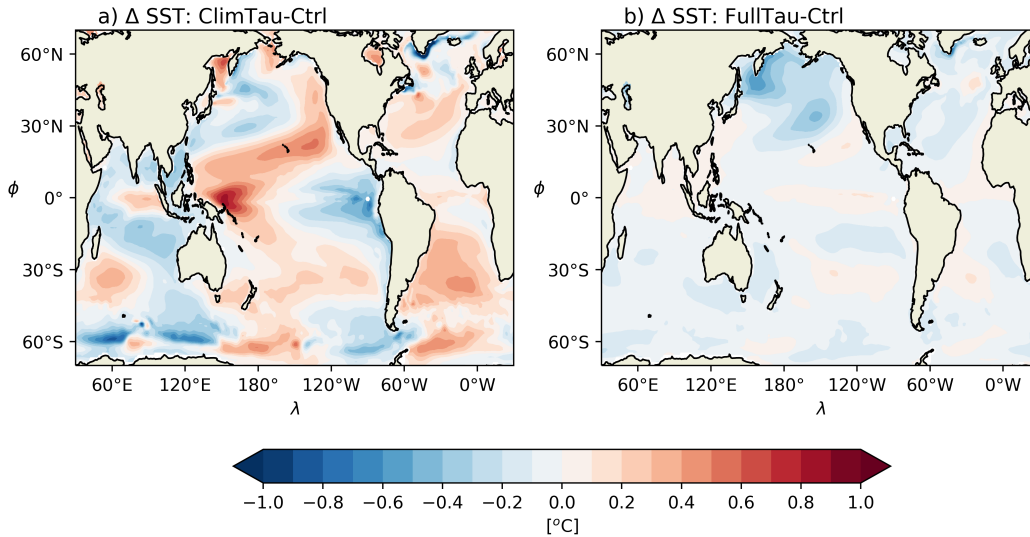


**Figure 4.** SST bias between (a) ClimTau and Ctrl and (b) FullTau and Ctrl averaged over the 50-year simulations.

204 The globally averaged SST time series of ClimTau and FullTau do not show ap-  
 205 preciable drift away from Ctrl (Figure S1). However, climatological decoupling creates  
 206 local SST residuals throughout the global oceans on the order of  $\pm 1^{\circ}\text{C}$  (Figure 4a). Note  
 207 that this pattern holds for seasonal averages as well (Figure S2). In contrast, the local  
 208 SST residuals created by interannually varying wind stress overriding (Figure 4b) are  
 209 considerably smaller, except for a patch of negative SST anomalies in the North Pacific  
 210 on the poleward side of the Aleutian low. This cool patch, which is significantly differ-  
 211 ent from Ctrl at the 95% level using a Student’s  $t$ -test, occurs in three ensemble mem-  
 212 bers (not shown), suggesting that it is a robust physical bias inherent to the FullTau set-  
 213 up. Regardless of what caused this cool patch— plausibly a change in the Kuroshio or  
 214 the disruption of the positive covariance between turbulent and Ekman fluxes in the North  
 215 Pacific westerly regime— the cooling can be communicated globally through atmospheric  
 216 processes. This may explain why outside of this cool patch, the FullTau biases are neg-

217 active nearly everywhere. The ClimTau SST biases, on the other hand, are significantly  
218 different from Ctrl at the 95% level across the entirety of the surface ocean (not shown)  
219 and consist of both positive and negative values. ClimTau SST biases in the North Pa-  
220 cific, the equatorial Indo-Pacific, the North Atlantic, and the Southern Ocean are par-  
221 ticularly noteworthy (Figure 4a). Note that although the deep ocean would continue to  
222 adjust for far longer than these 50-year simulations, these surface bias patterns are rel-  
223 atively steady and experience a drift of only  $< 0.005^{\circ}\text{C}/\text{yr}$  in the last 20 years of the  
224 50-year simulations (not shown).

225 The pattern and amplitude of the SST bias in the North Pacific is reminiscent of  
226 the positive phase of the Pacific Decadal Oscillation (PDO: Mantua & Hare, 2002), with  
227 cool SST anomalies in the Kuroshio Extension region and warm SST anomalies along  
228 the California coast. Larson et al. (2022) find a similar bias pattern between their fully  
229 coupled and climatological overriding simulations (their Figure 5). They use a third sim-  
230 ulation where climatological wind stress overriding is only applied in the Equatorial Pa-  
231 cific to show that this positive PDO-like SST pattern partially results from air-sea heat  
232 flux anomalies in the absence of ENSO. However, this difference only accounts for a por-  
233 tion of the bias observed in Larson et al. (2022), with the remaining SST bias attributed  
234 to non-ENSO momentum dynamics and air-sea heat fluxes. Because the act of wind stress  
235 overriding disables a coupled ENSO regardless of the methodology used, and because we  
236 only find this PDO-like SST bias pattern in ClimTau, the full bias discussed in Larson  
237 et al. (2022) may be partially explained as an artifact of the decoupling technique used.

238 The warm SST anomalies in ClimTau extend from the subtropics southwestward  
239 along the PMM path into the tropics, where the resemblance to the positive PDO is lost.  
240 In fact, the clear zonal SST dipole in the Equatorial Pacific is somewhat reminiscent of  
241 a negative PDO; the Western Equatorial Pacific (WEP) experiences relatively strong warm-  
242 ing and the Eastern Equatorial Pacific (EEP) experiences relatively strong cooling. Ogata  
243 et al. (2013) suggest that ENSO variability rectifies the interdecadal mean state of the  
244 tropical Pacific, and these biases may result from the lack of interannual variability in  
245 ClimTau because the SST bias pattern of warmer WEP and cooler EEP in ClimTau cor-  
246 responds to suppressed ENSO amplitude. Consistent with this, FullTau has ENSO-like  
247 interannual thermocline variability, although it does not have interactive ENSO, and it  
248 does not have these equatorial SST dipole biases. A similar zonal SST dipole exists in  
249 the Indian Ocean where the Eastern Indian Ocean warms and the Western Indian Ocean

250 cools. As a quantitative point of comparison, the EEP SST difference in ClimTau is of  
251 a similar magnitude as the EEP SST response found by Luongo et al. (2023), where the  
252 climate was forced by a strong insolation reduction in the region  $45^\circ - 65^\circ\text{N}$ . Despite  
253 a disabled Bjerknes feedback and even without canonical ENSO variability, these tropi-  
254 cal SST biases can still excite anomalous ocean circulation, turbulent heat fluxes at the  
255 ocean surface, and large-scale atmospheric circulation responses which can anchor these  
256 anomalies in place. In turn, these equatorial anomalies may then affect the subtropics  
257 via evaporative heat fluxes retained in mechanically decoupled simulations (e.g., Chiang  
258 & Vimont, 2004; Luongo et al., 2023), subsurface ocean ventilation (e.g., Burls et al., 2017;  
259 Heede et al., 2020), or changes in deep convection (e.g., Hoskins & Karoly, 1981).

260 The schematic of wind stress overriding in Figure 1 does not address how the wind  
261 stress is treated in regions that have sea ice, and neither wind stress overriding scheme  
262 perfectly deals with a potential climate jump at the sea ice edge. Comparison of ClimTau  
263 and FullTau SST residuals in the North Atlantic and Southern Ocean suggest that ClimTau  
264 SST biases in these regions, which exhibit a pronounced seasonality (Figure S2), are likely  
265 more complex than simply a result of sea ice effects. These anomalous SST patterns and  
266 resulting anomalous buoyancy fluxes cause ocean circulation adjustment and restrati-  
267 fication, including in areas of deep convection such as the Labrador and Weddell Seas.

268 Although the present analysis only focuses on wind stress overriding in coupled GCMs,  
269 it is worth briefly considering previous studies that used similar approaches in ocean-  
270 only GCMs. For instance, while many studies force ocean GCMs with a wind stress cli-  
271 matology (e.g., Peng et al., 2022), ocean-only FAFMIP (OFAFMIP: Todd et al., 2020)  
272 found that overriding with a climatology created biases relative to coupled GCM con-  
273 trol simulations and so instead specified interannually varying daily surface momentum  
274 fluxes. Similarly, a number of previous ocean-only GCM studies have looped the wind  
275 stress field from a specific year to investigate buoyancy impacts on ocean circulation (Luo  
276 et al., 2015; F. Liu et al., 2017). While this method maintains the effects of synoptic and  
277 subseasonal variability on the surface ocean, any peculiarities of the year chosen can strongly  
278 imprint on the mean simulated climate state. To explore the implications of using this  
279 as a coupled GCM overriding method, we take wind stress fields from a neutral, nega-  
280 tive, and positive ENSO year in Ctrl, as defined by the Nino 3.4 SST index (Figure S3a).  
281 We run three additional 50-year simulations, “ENSONeutralTau,” “ENSONegativeTau,”  
282 and “ENSOPositiveTau,” each forced by repeating the wind stress from a different sin-

283 gle year. SST biases using this overriding method are much larger than in either ClimTau  
 284 or FullTau (Figure S3b-g), and the specific patterns vary depending on which year is cho-  
 285 sen within an ENSO cycle. These results suggest that overriding with a single repeat-  
 286 ing year leads to strikingly large biases and does not accurately recreate the mean state  
 287 of the surface ocean.

### 288 **3.2 Possible Mechanisms for Bias in ClimTau**

The rate of kinetic energy input from winds into the surface ocean velocity field,  
 often called “wind work,” is given by the inner product of the wind stress and the sur-  
 face ocean velocity,

$$\Pi = \vec{\tau} \cdot \vec{u} . \quad (2)$$

289 Because the surface velocity field can be decomposed into geostrophic and ageostrophic  
 290 components,  $\vec{u} = \vec{u}_g + \vec{u}_{ag}$ ,  $\Pi$  can also be decomposed similarly,  $\Pi = \Pi_g + \Pi_{ag}$ .  $\Pi_g$  is a  
 291 main driver of large-scale ocean circulation and a major source of mechanical energy for  
 292 the deep ocean (e.g., Oort et al., 1994; Munk & Wunsch, 1998; Wunsch & Ferrari, 2004;  
 293 Ferrari & Wunsch, 2009). Wunsch (1998) used reanalysis winds and satellite altimeter  
 294 data to compute 10-day averages of  $\vec{\tau}$  and  $\vec{u}_g$  and solve for a global estimate of  $\Pi_g$  of about  
 295 1 TW. Subsequent studies have generally confirmed  $\Pi_g \approx 1$  TW and that most of this  
 296 work is done in the Southern Ocean by the zonal component of the time-averaged wind  
 297 stress on the time-averaged geostrophic surface velocity (Huang et al., 2006; Hughes &  
 298 Wilson, 2008; Scott & Xu, 2009; Zhai et al., 2012).

299 However, considering that synoptic storms make up some of the most prominent  
 300 peaks in the time series of  $\Pi$  (Alford, 2001),  $\Pi_{ag}$  associated with synoptic events likely  
 301 substantially contributes to global estimates of  $\Pi$ . Indeed, in GCM diagnoses, von Storch  
 302 et al. (2007) and Gregory and Tailleux (2011) used actual simulated  $\vec{\tau}$  and  $\vec{u}$  and eval-  
 303 uated total  $\Pi \approx 3 - 4$  TW, further establishing that only considering  $\Pi_g$  gives a sub-  
 304 stantial underestimate of total mechanical energy input to the surface ocean. Wang and  
 305 Huang (2004) use a classical Ekman spiral solution to solve for  $\Pi_{ag}$  and, in addition to  
 306 power estimates of near-inertial motions (e.g., Alford, 2001), suggest  $\Pi_{ag} \approx 2-3$  TW.  
 307 Elipot and Gille (2009) show that the primary contributor to  $\Pi_{ag}$  is the covariance of  
 308 wind stress and surface velocities and, according to Wang and Huang (2004),  $\Pi_{ag}$  is spent  
 309 supporting turbulence and mixing to maintain upper ocean velocity and stratification

310 fields. Because FullTau has a much larger wind stress variance than ClimTau (c.f. Fig-  
 311 ure 3a & b), FullTau should also have a larger  $\Pi_{ag}$  than ClimTau. While a full decom-  
 312 position into  $\Pi_g$  and  $\Pi_{ag}$  is beyond the scope of this work, Figure 3c presents the dif-  
 313 ference in total  $\Pi$  between FullTau and ClimTau and shows nearly uniform positive val-  
 314 ues poleward of the deep tropics. This difference between the two simulations likely re-  
 315 sults from the difference in  $\Pi_{ag}$  associated with the preservation of high frequency wind  
 316 stress variability (Figure 2b). In particular, FullTau experiences substantially more wind  
 317 work than ClimTau in regions with high wind stress variance such as the Southern Ocean  
 318 and the Northern Hemisphere storm tracks.

319 Figure 3c clearly shows that the lack of synoptic variability in ClimTau leads to  
 320 a less energetic surface ocean across much of the globe and therefore less energy avail-  
 321 able to sustain realistic levels of near-surface mixing. Indeed, the mixed layer depth (MLD)  
 322 in ClimTau is substantially shallower than Ctrl throughout much of the global ocean (Fig-  
 323 ure 5a). In particular, the mixed layer is biased too shallow in nearly all extratropical  
 324 regions outside of 30°S to 30°N. These MLD patterns qualitatively match the global pat-  
 325 tern of the daily wind stress variance and the difference in  $\Pi$  between FullTau and ClimTau  
 326 (Figure 3), indicating the critical role of synoptic variability in maintaining the MLD in  
 327 these extratropical regions.

328 Suppressed wind stress variance associated with winter and spring synoptic storms  
 329 seem to play a key role in the annual mean MLD response: the too shallow MLD sig-  
 330 nature in the Northern Hemisphere is strongest in boreal winter and spring, while the  
 331 too shallow MLD signature in the Southern Hemisphere is strongest in austral winter  
 332 and spring (Figure S4). The ClimTau MLD bias is smaller throughout much of the trop-  
 333 ics, which is also the region with the lowest daily wind stress variance (Figure 3a & b).  
 334 However, a shallow MLD signal does exist in the tropical Indo-Pacific around the mar-  
 335 itime continent in the ClimTau experiment, which may be locally related to disabled ENSO  
 336 variability or perhaps to the lack of synoptic tropical cyclone-like activity. On the other  
 337 hand, with the exception of the far North Atlantic, there are minimal differences between  
 338 MLD in FullTau and Ctrl throughout much of the ocean (Figure 5b). The too deep MLD  
 339 bias in the North Atlantic may result from changes in the AMOC caused by the lack of  
 340 covariance between the surface ocean and high frequency stochastic wind stress forcing  
 341 or from geographic shifts in the locations of deep convection.

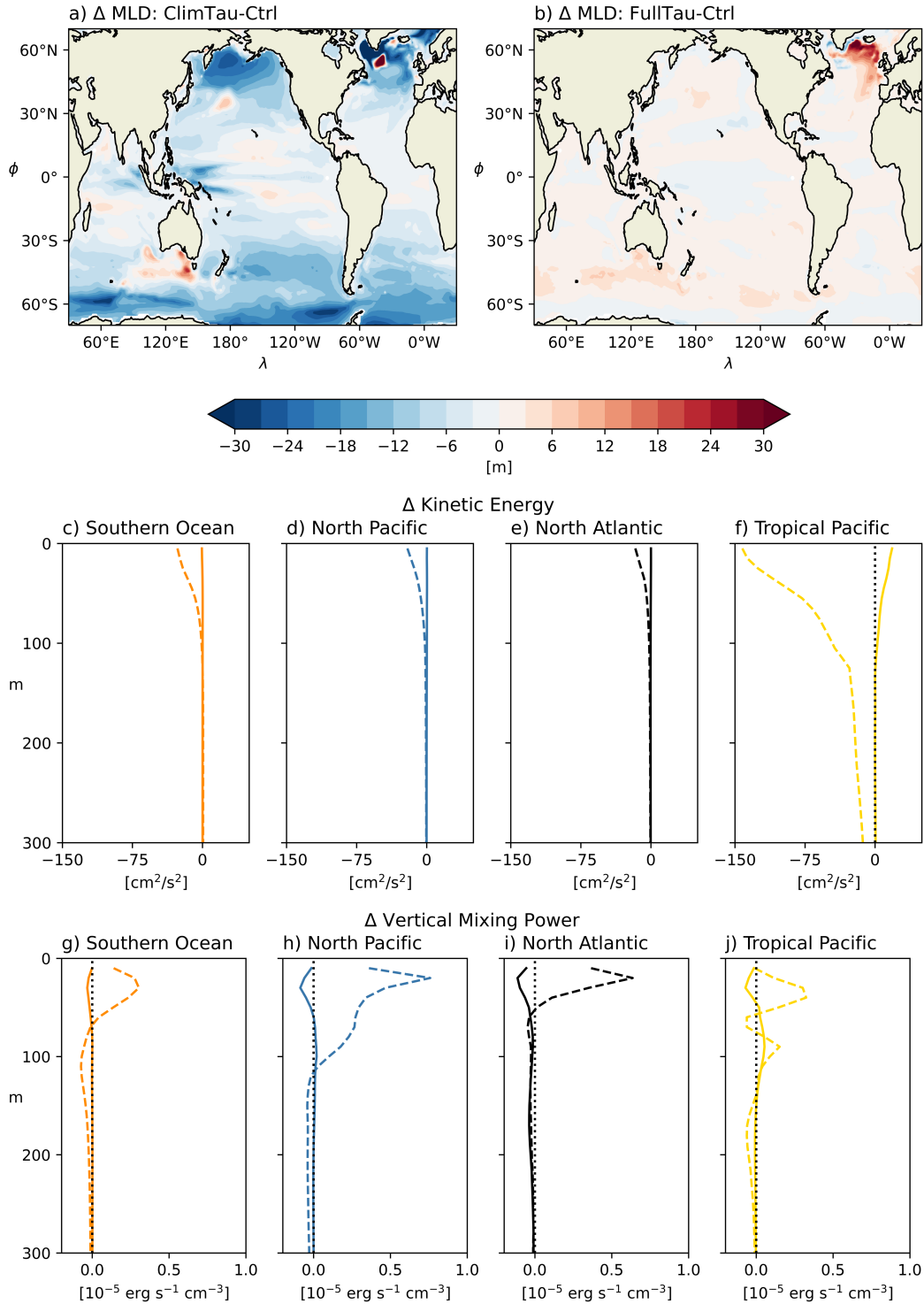


**Figure 5.** Top row: 50-year average mixed layer depth (MLD) bias between (a) ClimTau and Ctrl and (b) FullTau and Ctrl. Middle row: 50-year regional average depth profile of horizontal kinetic energy bias between ClimTau and Ctrl (dashed lines) and FullTau and Ctrl (solid lines). Bottom row: 50-year regional average depth profile of vertical mixing power bias between ClimTau and Ctrl (dashed lines) and FullTau and Ctrl (solid lines).

342 The lack of synoptic variability in ClimTau has a notable impact on area-averaged  
 343 depth profiles of near-surface horizontal kinetic energy biases. Figures 5c-f show that cli-  
 344 matological overriding causes a decrease in near-surface kinetic energy over the South-  
 345 ern Ocean (orange dashed line), North Pacific (blue dashed line), North Atlantic (black  
 346 dashed line), and tropical Pacific (dashed yellow line). In the extratropics, the negative  
 347 near-surface kinetic energy bias in ClimTau likely results from the decreased wind work  
 348 seen in Figure 3c. On the other hand, the decrease in tropical Pacific kinetic energy is  
 349 substantially larger than in the extratropical regions. Because ClimTau experiences smaller  
 350 wind stress variance biases in the tropics, this difference is likely primarily a result of re-  
 351 duced ENSO variability rather than reduced synoptic variability. Meanwhile, the differ-  
 352 ence in near-surface kinetic energy profiles between FullTau and Ctrl (Figure 5c-f: solid  
 353 lines, same colors) are near zero in non-tropical regions. In the tropical Pacific, however,  
 354 the difference in the kinetic energy bias profile is positive and nearly the same magni-  
 355 tude as ClimTau’s North Pacific bias. This may result from the disruption of the covari-  
 356 ance between wind stress and surface currents in the equatorial region, where surface cur-  
 357 rents can damp changes in wind stress (Seo et al., 2023). This bias is likely also related  
 358 to the decreased  $\Pi$  observed in the tropics in FullTau (Figure 3c). Though changes in  
 359 kinetic energy profiles could in principle be caused by factors other than changes in wind  
 360 stress (e.g., anomalous buoyancy fluxes), CESM diagnostically reports monthly total volume-  
 361 integrated kinetic energy, and changes to total kinetic energy from wind stress are con-  
 362 sistent an order of magnitude larger than other changes (not shown).

363 The decrease of wind work and near-surface kinetic energy in ClimTau is related  
 364 to changes in vertical mixing power (the “TPOWER” variable in CESM). CESM uses  
 365 the  $K$ -profile parameterization scheme (Large et al., 1994; Danabasoglu et al., 2006) to  
 366 solve for vertical mixing power as the product of parameterized vertical diffusivity, den-  
 367 sity, and the vertical buoyancy gradient. Here, diffusivity depends on atmospheric forc-  
 368 ing and near-surface ocean current shear such that changes in wind stress between Full-  
 369 Tau and ClimTau change both the flow field and the diffusivity and thereby change the  
 370 vertical mixing power. In turn, vertical mixing power is equal to the rate of work done  
 371 against gravity to transport buoyancy within the mixed layer to reduce the vertical buoy-  
 372 ancy gradient. Because heat absorbed by the ocean will stay close to the surface unless  
 373 mechanical energy stirs it deeper, a change in vertical mixing power will affect heat trans-  
 374 port between the surface mixed layer and the thermocline. Figures 5g-j show an increase

375 in vertical mixing power in ClimTau just below the surface in all regions and a decrease  
376 in vertical mixing power at greater depths. This response implies that most of the avail-  
377 able mixing energy in ClimTau is spent mixing areas near the surface which are largely  
378 homogeneous in FullTau and Ctrl. Meanwhile, decreased vertical mixing in the thermo-  
379 cline suggests less of a connection between the mixed layer and colder thermocline wa-  
380 ters below. Near-surface FullTau vertical mixing profile biases are slightly negative which  
381 may plausibly have to do with diffusivity changes as a result of the near-uniform cool-  
382 ing bias observed in FullTau (Figure 4b).

383 The bias toward too shallow MLD values in ClimTau has substantial implications  
384 for the surface ocean-atmosphere coupled system. By reducing the MLD, climatologi-  
385 cal wind stress overriding reduces the effective heat capacity of the surface ocean. The  
386 reduced effective heat capacity of the surface ocean is expected to reduce the coupling  
387 time scales between the atmosphere and ocean. Hence, the shallow MLD in ClimTau is  
388 expected to allow anomalous mixed layer heat to rapidly change SST locally, whereas  
389 the synoptic variability in Ctrl provides sufficient kinetic energy to mix anomalous heat  
390 into the thermocline. Anomalous SSTs in ClimTau may then trigger atmospheric responses  
391 which can amplify anomalies further. We note, for instance, the clear PMM patterns in  
392 both hemispheres of the subtropical Pacific (Figure 4a), where evaporative cooling dom-  
393 inates the surface heat budget, which persist throughout the year (Figure S2). SST anoma-  
394 lies in the extratropics, where synoptic variability is key to maintaining a realistic ocean  
395 state, can go on to affect the tropics, where synoptic variability may be less important,  
396 either through surface pathways mediated by cloud feedbacks and the Northern or South-  
397 ern PMM (e.g., Dong et al., 2022; Luongo et al., 2023) or through subsurface ocean cir-  
398 culation adjustment of the subtropical cells (Burls et al., 2017; Heede et al., 2020). Once  
399 in the tropics, SST anomalies can trigger anomalous deep convection and affect the ex-  
400 tratropics (Hoskins & Karoly, 1981). In addition, by not mixing as much heat into the  
401 thermocline, ClimTau likely differs from Ctrl in the amount of heat that could otherwise  
402 reemerge remotely through ocean dynamics (Jansen et al., 2010; Brizuela et al., 2023).  
403 Overall, we find that climatological wind stress overriding leads to a shallower MLD and  
404 a less energetic near-surface ocean such that anomalous heat fluxes into the mixed layer  
405 may be expected to affect SST more rapidly.

## 4 Discussion

In the preceding section, we showed that climatological wind stress overriding simulations develop spurious temperature responses due to insufficient wind-driven mechanical energy input into the near-surface ocean. Although some prior studies have shown the mean state climate biases generated by their choice of wind stress overriding technique, here we have systematically compared the magnitude and pattern of SST biases created by two methods of wind stress overriding. Through this comparison we highlighted important differences between the two methods, which may be useful to inform future overriding studies.

We emphasize two central points associated with these results. First, decoupling biases exist in all wind stress overriding studies regardless of the overriding technique used. This mean state bias is especially relevant whenever the mean state of a fully coupled simulation is compared with that of a mechanically decoupled simulation. A number of previous studies have based their conclusions on such comparisons. For example, F. Liu et al. (2021) heated the Southern Ocean in CESM1 and then compared the fully coupled response with the response from a simulation under the same forcing but with climatological wind stress overriding. The near-surface differences in temperature, which they ascribe to wind stress forcing, are smaller than the biases that we find to be introduced via climatological overriding (c.f. Figure 4a with their Figure 8). In a similar vein, McMonigal et al. (2023) simulate greenhouse warming in CESM2 with and without climatological wind stress overriding and conclude that wind-driven changes accelerate greenhouse warming. Although their overriding bias pattern, defined here as their unforced mechanically decoupled simulation minus their unforced control simulation, differs from what we find in CESM1 (c.f. Figure 4a with their Figure S1 with the sign reversed), in general their bias show a nearly-uniform warming of around  $1^{\circ}\text{C}$ , which is the same order as what they attribute to the role of wind stress forcing in greenhouse warming (their Figure 4).

This bias can be explained using a simple example. Consider a situation where greenhouse forcing is applied in a fully coupled CESM1 simulation and that simulation is then compared with a simulation that has the same greenhouse forcing but overrides wind stress with the interannually varying wind stress from an unforced control simulation. If we compared these two simulations directly, the near uniform cooling seen in Figure 4b would

438 project onto what would be considered the forced response. This would add a near uni-  
439 form warming of the globe to the actual effect of wind stress changes associated with global  
440 warming. In other words, part of the simulated signal would be a spurious decoupling  
441 bias. Similarly, if the same analysis is instead carried out using climatological wind stress  
442 overriding [as in F. Liu et al. (2021) and McMonigal et al. (2023)], the spurious tropi-  
443 cal Pacific zonal dipole biases in Figure 4a would be added to the actual effect of wind  
444 stress changes. This could readily lead to inaccurate conclusions regarding the tropical  
445 response associated with global warming. When exploring an externally forced response,  
446 such as greenhouse or aerosol forcing, a direct way to address this issue of mean state  
447 bias is by comparing two mechanically decoupled simulations. To the extent that the sys-  
448 tem responds linearly, differencing a mechanically decoupled simulation from another me-  
449 chanically decoupled simulation will remove mean state biases. This method of compar-  
450 ing a forced mechanically decoupled simulation with an unforced mechanically decou-  
451 pled control was suggested by Lu and Zhao (2012) and adopted in some subsequent stud-  
452 ies (W. Liu et al., 2015, 2018; Luongo et al., 2022a, 2023; Fu & Fedorov, 2023).

453 The second central point relates to the potential impact of wind stress overriding  
454 mean state biases on climate variability: decoupling biases in the mean state can have  
455 major global impacts if they affect large-scale modes of variability (e.g., Richter et al.,  
456 2018). For instance, ClimTau mean state biases are most strikingly different from Full-  
457 Tau in the tropical Pacific, where there is an approximately  $2^{\circ}\text{C}$  spurious zonal temper-  
458 ature gradient. This ENSO-like zonal dipole has been observed to arise from decadal at-  
459 mospheric forcing of slab ocean simulations (Clement et al., 2011; Okumura, 2013) and  
460 can then affect extratropical variability through atmospheric teleconnections. As such,  
461 in studies which have used wind stress overriding to investigate internal variability out-  
462 side of the Equatorial Pacific (e.g., Larson, Vimont, et al., 2018; Zhang et al., 2021; Lar-  
463 son et al., 2022), tropical SST biases from overriding may alter extratropical variabil-  
464 ity in a way that is not equivalent to what could be ascribed to ENSO forcing alone. This  
465 suggests that the difference between climate variability in a fully coupled simulation and  
466 a climatological overriding simulation can not be interpreted as entirely attributable to  
467 the effect of ENSO on the climate system. Instead, differences may be a combination of  
468 both ENSO forcing and how these spurious effects of decoupling impact climate variabil-  
469 ity, and pinpointing exactly which of these responses dominates requires careful exper-  
470 imental design. Though this second consideration is relevant to all wind stress overrid-

471 ing simulations, it is reasonable to assume that reducing biases as much as possible helps  
472 with this issue.

473 Although we find that climatological wind stress overriding produces substantially  
474 larger biases than interannually varying wind stress overriding when compared with a  
475 control simulation, we note that there are situations where climatological wind stress over-  
476 riding is preferable to interannually varying wind stress overriding. For instance, inter-  
477 annual wind stress variability in the prescribed wind stress field can still affect the ther-  
478 moclone to create an uncoupled ENSO-like response in the interannually varying over-  
479 riding scheme. As result, interannually varying overriding would be an inappropriate tool  
480 to remove ENSO variability as initially accomplished by Larson and Kirtman (2015). Be-  
481 cause the two methods are only interchangeable in so far as they both disable momen-  
482 tum feedbacks between the atmosphere and ocean, the ultimate choice of wind stress over-  
483 riding technique depends on the scientific question at hand. In general, climatological  
484 overriding works well for scientific questions which depend on the mean wind stress sea-  
485 sonal cycle and where higher frequency variability obscures the signal [e.g., the role of  
486 instabilities in ENSO initiation (Larson & Kirtman, 2015, 2017, 2019)]. On the other  
487 hand, interannually varying overriding works well for scientific questions which require  
488 a realistic upper ocean state or smaller decoupling biases.

## 489 **5 Conclusion**

490 In this study we investigate the biases generated in wind stress overriding simu-  
491 lations where the atmosphere is mechanically decoupled from the ocean in a coupled GCM.  
492 We find that the biases relative to a fully coupled control simulation in a mechanically  
493 decoupled simulation with climatological wind stress overriding are substantially larger  
494 than the biases in a mechanically decoupled simulation which uses interannually vary-  
495 ing overriding. The climatological wind stress overriding biases take the form of famil-  
496 iar patterns of surface ocean and atmosphere variability, such as meridional modes and  
497 atmospherically forced ENSO-like and Indian Ocean Dipole-like zonal dipoles. However,  
498 these bias patterns are absent in the simulations with interannually varying wind stress  
499 overriding, showing that these biases do not merely represent the influence of momen-  
500 tum coupling on the surface ocean. These biases are present in past climatological wind  
501 stress overriding studies and are especially relevant when comparing the forced response

502 of a fully coupled and mechanically decoupled simulation and if the mean state biases  
503 appreciably affect extratropical climate variability.

504 Although we focus on SST residuals in this study, similar differences occur in other  
505 climate variables as well (e.g., net surface heat flux, precipitation, and sea level pressure;  
506 not shown). We find that the substantial bias in climatological overriding occurs because  
507 climatological overriding removes synoptic and subseasonal variability. This lack of high  
508 frequency variability in the climatological wind stress overriding simulations leads to shoal-  
509 ing of the ocean mixed layer throughout the extratropical region, which otherwise ex-  
510periences high day-to-day wind stress variance. We find that the near-surface ocean in  
511 climatological overriding simulations is characterized by reduced kinetic energy, too much  
512 vertical mixing at the surface, and not enough vertical mixing at depth.

513 While simulations forced with climatological wind stress were initially used as an  
514 effective means to remove the influence of ENSO on the climate, many subsequent stud-  
515ies have used climatological overriding to study extratropical variability and forced cli-  
516mate responses. As measured by the size of the bias compared with a fully coupled sim-  
517ulation, the results of the present study suggest that climatological overriding does not  
518create as realistic of an ocean state as when an interannually varying wind stress field  
519is used. We find that climatological overriding adds SST biases on the order of  $\pm 1^\circ\text{C}$  through-  
520out the global ocean while interannually varying overriding leads to considerably smaller  
521biases nearly everywhere. By directly comparing these two overriding methods, we em-  
522phasize the importance of matching the overriding technique with the scientific question  
523at hand to minimize the impact of decoupling effects on the scientific phenomenon be-  
524ing investigated. These results provide context for potential reinterpretation of past cli-  
525matological overriding studies and lay a foundation for future wind stress overriding stud-  
526ies and their bias tolerance.

## 527 **6 Open Research**

528 The interannually varying wind stress overriding protocol for CESM is available  
529 through the UCSD library digital collections (Luongo et al., 2022b). The climatologi-  
530cal overriding protocol will be hosted by the UCSD library digital collections upon study  
531 publication. The data used to create Figures 2-5 have been uploaded for this initial sub-

532 mission as .mat files; they will be made freely available from the UCSD library digital  
533 collections upon publication.

### 534 **Acknowledgments**

535 This work was supported by NASA FINESST Fellowship 80NSSC22K1528 and NSF grant  
536 OCE-2048590. We thank UCAR and NSF for providing the graduate student allocation  
537 of core hours on Cheyenne that this research used and we thank the Extratropical-Tropical  
538 Interaction Model Intercomparison Project group for making their restart files available.  
539 Without implying their endorsement, we thank Clara Deser, Matthew H. Alford, Momme  
540 Hell, and Bruce Cornuelle for helpful discussions and suggestions. We also thank our ed-  
541 itor, Dr. Stephen Griffies, and three anonymous reviewers for their thoughtful and con-  
542 structive feedback which greatly improved this study.

### 543 **References**

- 544 Alford, M. H. (2001). Internal swell generation: The spatial distribution of en-  
545 ergy flux from the wind to mixed layer near-inertial motions. *Journal of Physi-  
546 cal Oceanography*, *31*(8), 2359–2368.
- 547 Bjerknes, J. (1969). Atmospheric teleconnections from the equatorial Pacific.  
548 *Monthly Weather Review*, *97*(3), 163–172.
- 549 Brizuela, N. G., Alford, M. H., Xie, S.-P., Sprintall, J., Voet, G., Warner, S. J., . . .  
550 Moum, J. N. (2023). Prolonged thermocline warming by near-inertial internal  
551 waves in the wakes of tropical cyclones. *Proceedings of the National Academy  
552 of Sciences*, *120*(26), e2301664120.
- 553 Burls, N. J., Muir, L., Vincent, E. M., & Fedorov, A. (2017). Extra-tropical origin of  
554 equatorial Pacific cold bias in climate models with links to cloud albedo. *Cli-  
555 mate Dynamics*, *49*(5), 2093–2113.
- 556 Chakravorty, S., Perez, R. C., Anderson, B. T., Giese, B. S., Larson, S. M., & Piv-  
557 otti, V. (2020). Testing the trade wind charging mechanism and its influence  
558 on ENSO variability. *Journal of Climate*, *33*(17), 7391–7411.
- 559 Chakravorty, S., Perez, R. C., Anderson, B. T., Larson, S. M., Giese, B. S., & Piv-  
560 otti, V. (2021). Ocean dynamics are key to extratropical forcing of El Niño.  
561 *Journal of Climate*, *34*(21), 8739–8753.
- 562 Chiang, J. C., & Vimont, D. J. (2004). Analogous Pacific and Atlantic meridional

- 563 modes of tropical atmosphere–ocean variability. *Journal of Climate*, *17*(21),  
 564 4143–4158.
- 565 Clement, A., DiNezio, P., & Deser, C. (2011). Rethinking the ocean’s role in the  
 566 Southern Oscillation. *Journal of Climate*, *24*(15), 4056–4072.
- 567 Craig, A. (2014). CPL7 user’s guide. *Updated for CESM version*, *1*(6).
- 568 Danabasoglu, G., Large, W. G., Tribbia, J. J., Gent, P. R., Briegleb, B. P., &  
 569 McWilliams, J. C. (2006). Diurnal coupling in the tropical oceans of CCSM3.  
 570 *Journal of Climate*, *19*(11), 2347–2365.
- 571 Dong, Y., Armour, K. C., Battisti, D. S., & Blanchard-Wrigglesworth, E. (2022).  
 572 Two-way teleconnections between the Southern Ocean and the tropical Pacific  
 573 via a dynamic feedback. *Journal of Climate*, *35*(19), 6267–6282.
- 574 Eisenman, I. (2012). Factors controlling the bifurcation structure of sea ice retreat.  
 575 *Journal of Geophysical Research: Atmospheres*, *117*(D1).
- 576 Elipot, S., & Gille, S. T. (2009). Estimates of wind energy input to the Ekman  
 577 layer in the Southern Ocean from surface drifter data. *Journal of Geophysical  
 578 Research: Oceans*, *114*(C6).
- 579 Ferrari, R., & Wunsch, C. (2009). Ocean circulation kinetic energy: Reservoirs,  
 580 sources, and sinks. *Annual Review of Fluid Mechanics*, *41*(1), 253–282.
- 581 Fu, M., & Fedorov, A. (2023). The role of Bjerknes and shortwave feedbacks in the  
 582 tropical Pacific SST response to global warming. *Geophysical Research Letters*,  
 583 *50*(19), e2023GL105061.
- 584 Green, B., & Marshall, J. (2017). Coupling of trade winds with ocean circulation  
 585 damps ITCZ shifts. *Journal of Climate*, *30*(12), 4395–4411.
- 586 Gregory, J. M., Bouttes, N., Griffies, S. M., Haak, H., Hurlin, W. J., Jungclaus, J.,  
 587 ... others (2016). The flux-anomaly-forced model intercomparison project  
 588 (FAFMIP) contribution to CMIP6: Investigation of sea-level and ocean climate  
 589 change in response to CO<sub>2</sub> forcing. *Geoscientific Model Development*, *9*(11),  
 590 3993–4017.
- 591 Gregory, J. M., & Tailleux, R. (2011). Kinetic energy analysis of the response of the  
 592 Atlantic meridional overturning circulation to CO<sub>2</sub>-forced climate change. *Cli-  
 593 mate Dynamics*, *37*, 893–914.
- 594 Heede, U. K., Fedorov, A. V., & Burls, N. J. (2020). Time scales and mechanisms  
 595 for the tropical Pacific response to global warming: A tug of war between the

- 596 ocean thermostat and weaker Walker. *Journal of Climate*, *33*(14), 6101–6118.
- 597 Held, I. M. (2005). The gap between simulation and understanding in climate mod-  
 598 eling. *Bulletin of the American Meteorological Society*, *86*(11), 1609–1614.
- 599 Holland, M. M., Bailey, D. A., Briegleb, B. P., Light, B., & Hunke, E. (2012). Im-  
 600 proved sea ice shortwave radiation physics in CCSM4: The impact of melt  
 601 ponds and aerosols on Arctic sea ice. *Journal of Climate*, *25*(5), 1413–1430.
- 602 Hoskins, B. J., & Karoly, D. J. (1981). The steady linear response of a spherical at-  
 603 mosphere to thermal and orographic forcing. *Journal of the Atmospheric Sci-*  
 604 *ences*, *38*(6), 1179–1196.
- 605 Huang, R. X., Wang, W., & Liu, L. L. (2006). Decadal variability of wind-energy  
 606 input to the world ocean. *Deep Sea Research Part II: Topical Studies in*  
 607 *Oceanography*, *53*(1-2), 31–41.
- 608 Hughes, C. W., & Wilson, C. (2008). Wind work on the geostrophic ocean circu-  
 609 lation: An observational study of the effect of small scales in the wind stress.  
 610 *Journal of Geophysical Research: Oceans*, *113*(C2).
- 611 Hurrell, J. W., Holland, M. M., Gent, P. R., Ghan, S., Kay, J. E., Kushner, P. J.,  
 612 ... others (2013). The Community Earth System Model: a framework for  
 613 collaborative research. *Bulletin of the American Meteorological Society*, *94*(9),  
 614 1339–1360.
- 615 Huybers, P., & Wunsch, C. (2003). Rectification and precession signals in the cli-  
 616 mate system. *Geophysical Research Letters*, *30*(19).
- 617 Jansen, M. F., Ferrari, R., & Mooring, T. A. (2010). Seasonal versus permanent  
 618 thermocline warming by tropical cyclones. *Geophysical Research Letters*,  
 619 *37*(3).
- 620 Kang, S. M., Xie, S.-P., Shin, Y., Kim, H., Hwang, Y.-T., Stuecker, M. F., ...  
 621 Hawcroft, M. (2020). Walker circulation response to extratropical radiative  
 622 forcing. *Science Advances*, *6*(47), eabd3021.
- 623 Large, W. G., McWilliams, J. C., & Doney, S. C. (1994). Oceanic vertical mixing: A  
 624 review and a model with a nonlocal boundary layer parameterization. *Reviews*  
 625 *of geophysics*, *32*(4), 363–403.
- 626 Larson, S. M., Buckley, M. W., & Clement, A. C. (2020). Extracting the buoyancy-  
 627 driven Atlantic meridional overturning circulation. *Journal of Climate*, *33*(11),  
 628 4697–4714.

- 629 Larson, S. M., & Kirtman, B. P. (2015). Revisiting ENSO coupled instability theory  
630 and SST error growth in a fully coupled model. *Journal of Climate*, *28*(12),  
631 4724–4742.
- 632 Larson, S. M., & Kirtman, B. P. (2017). Drivers of coupled model ENSO error dy-  
633 namics and the spring predictability barrier. *Climate Dynamics*, *48*(11), 3631–  
634 3644.
- 635 Larson, S. M., & Kirtman, B. P. (2019). Linking preconditioning to extreme ENSO  
636 events and reduced ensemble spread. *Climate Dynamics*, *52*(12), 7417–7433.
- 637 Larson, S. M., Kirtman, B. P., & Vimont, D. J. (2017). A framework to decompose  
638 wind-driven biases in climate models applied to CCSM/CESM in the eastern  
639 Pacific. *Journal of Climate*, *30*(21), 8763–8782.
- 640 Larson, S. M., Okumura, Y., Bellomo, K., & Breeden, M. L. (2022). Destructive  
641 interference of ENSO on North Pacific SST and North American precipita-  
642 tion associated with Aleutian low variability. *Journal of Climate*, *35*(11),  
643 3567–3585.
- 644 Larson, S. M., Pegion, K. V., & Kirtman, B. P. (2018). The South Pacific merid-  
645 ional mode as a thermally driven source of ENSO amplitude modulation and  
646 uncertainty. *Journal of Climate*, *31*(13), 5127–5145.
- 647 Larson, S. M., Vimont, D. J., Clement, A. C., & Kirtman, B. P. (2018). How  
648 momentum coupling affects SST variance and large-scale Pacific climate vari-  
649 ability in CESM. *Journal of Climate*, *31*(7), 2927–2944.
- 650 Lawrence, D. M., Oleson, K. W., Flanner, M. G., Fletcher, C. G., Lawrence, P. J.,  
651 Levis, S., . . . Bonan, G. B. (2012). The CCSM4 land simulation, 1850–2005:  
652 Assessment of surface climate and new capabilities. *Journal of Climate*, *25*(7),  
653 2240–2260.
- 654 Liu, F., Luo, Y., Lu, J., & Wan, X. (2017). Response of the tropical Pacific Ocean  
655 to El Niño versus global warming. *Climate Dynamics*, *48*(3), 935–956.
- 656 Liu, F., Luo, Y., Lu, J., & Wan, X. (2021). The role of ocean dynamics in the cross-  
657 equatorial energy transport under a thermal forcing in the southern ocean. *Ad-  
658 vances in Atmospheric Sciences*, *38*, 1737–1749.
- 659 Liu, W., Lu, J., & Xie, S.-P. (2015). Understanding the Indian Ocean response to  
660 double CO<sub>2</sub> forcing in a coupled model. *Ocean Dynamics*, *65*(7), 1037–1046.
- 661 Liu, W., Lu, J., Xie, S.-P., & Fedorov, A. (2018). Southern Ocean heat uptake,

- 662 redistribution, and storage in a warming climate: The role of meridional over-  
 663 turning circulation. *Journal of Climate*, 31(12), 4727–4743.
- 664 Lu, J., & Zhao, B. (2012). The role of oceanic feedback in the climate response to  
 665 doubling CO<sub>2</sub>. *Journal of Climate*, 25(21), 7544–7563.
- 666 Luo, Y., Lu, J., Liu, F., & Liu, W. (2015). Understanding the El Niño-like oceanic  
 667 response in the tropical Pacific to global warming. *Climate Dynamics*, 45(7),  
 668 1945–1964.
- 669 Luongo, M. T., Xie, S.-P., & Eisenman, I. (2022a). Buoyancy forcing dominates  
 670 the cross-equatorial ocean heat transport response to northern hemisphere  
 671 extratropical cooling. *Journal of Climate*, 35(20), 3071–3090.
- 672 Luongo, M. T., Xie, S.-P., & Eisenman, I. (2022b). *Data and Code from: Buoyancy*  
 673 *Forcing Dominates the Cross-Equatorial Ocean Heat Transport Response to*  
 674 *Northern Hemisphere Extratropical Cooling*. [CODE]. UC San Diego Digital  
 675 Collections. doi: <https://doi.org/10.6075/J0PR7W6B>
- 676 Luongo, M. T., Xie, S.-P., Eisenman, I., Hwang, Y.-T., & Tseng, H.-Y. (2023). A  
 677 Pathway for Northern Hemisphere Extratropical Cooling to Elicit a Tropical  
 678 Response. *Geophysical Research Letters*, 50(2), e2022GL100719.
- 679 Mantua, N. J., & Hare, S. R. (2002). The Pacific decadal oscillation. *Journal of*  
 680 *Oceanography*, 58(1), 35–44.
- 681 McMonigal, K., Larson, S., Hu, S., & Kramer, R. (2023). Historical Changes in  
 682 Wind-Driven Ocean Circulation Can Accelerate Global Warming. *Geophysical*  
 683 *Research Letters*, 50(4), e2023GL102846.
- 684 McMonigal, K., & Larson, S. M. (2022). ENSO Explains the Link Between Indian  
 685 Ocean Dipole and Meridional Ocean Heat Transport. *Geophysical Research*  
 686 *Letters*, 49(2), e2021GL095796.
- 687 Munk, W., & Wunsch, C. (1998). Abyssal recipes II: Energetics of tidal and wind  
 688 mixing. *Deep Sea Research Part I: Oceanographic Research Papers*, 45(12),  
 689 1977–2010.
- 690 Neale, R. B., Chen, C.-C., Gettelman, A., Lauritzen, P. H., Park, S., Williamson,  
 691 D. L., ... others (2010). Description of the NCAR community atmosphere  
 692 model (CAM 5.0). *NCAR Tech. Note NCAR/TN-486+ STR*, 1(1), 1–12.
- 693 Ogata, T., Xie, S.-P., Wittenberg, A., & Sun, D.-Z. (2013). Interdecadal amplitude  
 694 modulation of El Niño–Southern Oscillation and its impact on tropical Pacific

- 695 decadal variability. *Journal of Climate*, *26*(18), 7280–7297.
- 696 Okumura, Y. M. (2013). Origins of tropical Pacific decadal variability: Role of  
 697 stochastic atmospheric forcing from the South Pacific. *Journal of Climate*,  
 698 *26*(24), 9791–9796.
- 699 Oort, A. H., Anderson, L. A., & Peixoto, J. P. (1994). Estimates of the energy cycle  
 700 of the oceans. *Journal of Geophysical Research: Oceans*, *99*(C4), 7665–7688.
- 701 Peng, Q., Xie, S.-P., Wang, D., Huang, R. X., Chen, G., Shu, Y., . . . Liu, W. (2022).  
 702 Surface warming-induced global acceleration of upper ocean currents. *Science*  
 703 *Advances*, *8*(16), eabj8394.
- 704 Richter, I., Doi, T., Behera, S. K., & Keenlyside, N. (2018). On the link between  
 705 mean state biases and prediction skill in the tropics: an atmospheric perspec-  
 706 tive. *Climate Dynamics*, *50*, 3355–3374.
- 707 Scott, R. B., & Xu, Y. (2009). An update on the wind power input to the surface  
 708 geostrophic flow of the world ocean. *Deep Sea Research Part I: Oceanographic*  
 709 *Research Papers*, *56*(3), 295–304.
- 710 Seo, H., O’Neill, L. W., Bourassa, M. A., Czaja, A., Drushka, K., Edson, J. B., . . .  
 711 others (2023). Ocean Mesoscale and Frontal-Scale Ocean–Atmosphere Inter-  
 712 actions and Influence on Large-Scale Climate: A Review. *Journal of Climate*,  
 713 *36*(7), 1981–2013.
- 714 Smith, R., Jones, P., Briegleb, B., Bryan, F., Danabasoglu, G., Dennis, J., . . . others  
 715 (2010). The parallel ocean program (POP) reference manual ocean component  
 716 of the community climate system model (CCSM) and community earth system  
 717 model (CESM). *LAUR-01853*, *141*, 1–140.
- 718 Todd, A., Zanna, L., Couldrey, M., Gregory, J., Wu, Q., Church, J. A., . . . others  
 719 (2020). Ocean-only FAFMIP: Understanding regional patterns of ocean heat  
 720 content and dynamic sea level change. *Journal of Advances in Modeling Earth*  
 721 *Systems*, *12*(8), e2019MS002027.
- 722 von Storch, J.-S., Sasaki, H., & Marotzke, J. (2007). Wind-generated power input to  
 723 the deep ocean: An estimate using a  $1/10^\circ$  general circulation model. *Journal*  
 724 *of Physical Oceanography*, *37*(3), 657–672.
- 725 Wang, W., & Huang, R. X. (2004). Wind energy input to the Ekman layer. *Journal*  
 726 *of Physical Oceanography*, *34*(5), 1267–1275.
- 727 Wunsch, C. (1998). The work done by the wind on the oceanic general circulation.

- 728 *Journal of Physical Oceanography*, 28(11), 2332–2340.
- 729 Wunsch, C., & Ferrari, R. (2004). Vertical mixing, energy, and the general circula-  
730 tion of the oceans. *Annu. Rev. Fluid Mech.*, 36, 281–314.
- 731 Wyrтки, K. (1975). El Niño—the dynamic response of the equatorial Pacific Ocean  
732 to atmospheric forcing. *Journal of Physical Oceanography*, 5(4), 572–584.
- 733 Zhai, X., Johnson, H. L., Marshall, D. P., & Wunsch, C. (2012). On the wind power  
734 input to the ocean general circulation. *Journal of Physical Oceanography*,  
735 42(8), 1357–1365.
- 736 Zhang, Y., Yu, S., Amaya, D. J., Kosaka, Y., Larson, S. M., Wang, X., ... others  
737 (2021). Pacific meridional modes without equatorial Pacific influence. *Journal*  
738 *of Climate*, 34(13), 5285–5301.